Available online at www.sciencedirect.com
ScienceDirect
Vision Research 47 (2007) 834–844
Vision Research
www.elsevier.com/locate/visres

The spatial feature underlying the shape-frequency and shape-amplitude after-effects

Elena Gheorghiu *, Frederick A.A. Kingdom

McGill Vision Research, Department of Ophthalmology, McGill University, 687 Pine Avenue W., Montreal, Que., Canada H3A 1A1

Received 25 July 2006; received in revised form 6 November 2006

Abstract

The shape-frequency and shape-amplitude after-effects, or SFAE and SAAE, refer respectively to the shifts observed in the perceived shape-frequency and shape-amplitude of a sinusoidal test contour following adaptation to a similar-shaped contour. As with other shape after-effects the shifts are in a direction away from that of the adapting stimulus. Using a variety of procedures we tested whether the spatial feature that was adapted in the SFAE and SAAE was (a) local orientation, (b) average unsigned curvature, (c) periodicity/density, (d) shape-amplitude and (e) local curvature. Our results suggest that the last of these, local curvature, underlies both the SFAE and SAAE. The evidence in favour of local curvature was that the after-effect reached its maximum value when just half-a-cycle of the test contour, in ±cosine phase, was present. We suggest that the SFAE and SAAE are mediated by intermediate-level mechanisms that encode the shapes of contour fragments with constant sign of curvature. Given the neurophysiological evidence that neurons in area V4 encode parts of shapes with constant sign of curvature, we suggest V4 is the likely neural substrate for both the SFAE and SAAE.

Keywords: Contour-shape; Adaptation; Shape-frequency after-effect; Shape-amplitude after-effect; Curvature; Tilt after-effect

1. Introduction

Neurophysiological and psychophysical studies have shown that shape encoding mechanisms are located at various levels in the visual cortex, from oriented line and edge detectors in V1 (DeValois & DeValois, 1988; Hubel & Wiesel, 1968; Wilson, 1991), to curvature-sensitive detectors in V1 and V2 (Koenderink & Richards, 1988; Wilson & Richards, 1989), to parts of shape detectors in V4 (Gallant, Braun, & Van Essen, 1993; Gallant, Connor, Rakshit, Lewis, & Van Essen, 1996; Habak, Wilkinson, Zahker, & Wilson, 2004; Keeble & Hess, 1999; Levi & Klein, 2000; Pasupathy & Connor, 2002; Regan & Hamstra, 1992) and finally to whole-shape detectors in IT and LOC (Gross, 1992; Ito, Fujita, Tamura, & Tanaka, 1994; Tanaka, 1996).

Much of the psychophysical research on shape processing has involved the measurement of thresholds for detecting and discriminating simple shapes such as sinusoidal contours (Tyler, 1973), curved contours (Kramer & Fahle, 1996; Watt & Andrews, 1982; Wilson & Richards, 1989, 1992), chevrons (Wilson, 1986), radial frequency patterns (Habak et al., 2004; Hess, Wang, & Dakin, 1999; Loffler, Wilson, & Wilkinson, 2003; Wilkinson, Wilson, & Habak, 1998), ellipses and squares (Regan & Hamstra, 1992). Another approach to the study of shape processing is to use shape after-effects (Anderson, Habak, Wilkinson, & Wilson, 2005; Anderson & Wilson, 2005; Blakemore & Over, 1974; Coltheart, 1971; Gheorghiu & Kingdom, 2006a, 2006b; Regan & Hamstra, 1992; Riggs, 1973; Stromeyer & Riggs, 1974; Suzuki, 2001, 2003; Suzuki & Cavanagh, 1998). A shape after-effect is said to occur when adaptation to a shape alters the perceived shape of a subsequently presented test pattern. One of the earliest studies of a shape after-effect was Blakemore and Over's (1974) study of the curvature after-effect, in which adaptation to a curved line results in a straight line appearing curved in the opposite direction. Blakemore and Over showed that

* Corresponding author.
E-mail address: elena.gheorghiu@mcgill.ca (E. Gheorghiu).

0042-6989/$ - see front matter © 2006 Elsevier Ltd. All rights reserved.
doi:10.1016/j.visres.2006.11.023

the curvature after-effect in fact resulted from local orientation adaptation, in other words from multiple tilt after-effects (TAEs), rather than curvature adaptation per se. Their study is instructive because it advises caution when attributing a shape after-effect to processes beyond local orientation adaptation. Nevertheless, several recent studies have argued that some shape after-effects occur at the level of global shape processing, i.e. beyond the stage of orientation adaptation, because they transfer across size and/or position (Anderson et al., 2005; Regan & Hamstra, 1992; Suzuki & Cavanagh, 1998) or are attention-dependent (Suzuki, 2001, 2003).

Recently, Kingdom and collaborators (Gheorghiu & Kingdom, 2006a, 2006b; Kingdom & Prins, 2005a, 2005b) demonstrated a shape after-effect termed the 'shape-frequency after-effect', or SFAE, in which adaptation to a sine-wave-shaped contour produces a shift in the apparent shape-frequency of a test contour in a direction away from that of the adapting stimulus. An important property of the SFAE is that it occurs even when the shape-phase of the adaptor is randomly changed every half second during the adaptation period, suggesting that the SFAE is unlikely to be due to local orientation adaptation (though as we shall see, one cannot rule this out a priori). We have also recently introduced the amplitude analog of the SFAE—the shape-amplitude after-effect, or SAAE (Kingdom & Gheorghiu, 2006)—in which the shape-amplitude of a sine-wave-shaped contour is perceived shifted in a direction away from that of the adapting stimulus. The reader can experience the SFAE and the SAAE in Fig. 1a and b. Non-static-adaptor versions can be viewed on http://www.mvr.mcgill.ca/Fred/research.htm#contourShapePerception.

The aim of the present study is to determine which spatial feature(s) underlies the SFAE and SAAE. At issue here is not so much the mechanism of adaptation per se, but the spatial feature(s) of the sine-wave contour that is being adapted, e.g. whether it is local orientation, local curvature, global shape etc. It is important to know which feature(s) is being adapted if the SFAE and SAAE are to be used to study shape processing.

The general procedure we have employed is to present subjects with pairs of adaptors that differ by a factor of three in either shape-frequency or shape-amplitude, and ask subjects to adjust the difference between two test stimuli presented at the same retinal locations as the adaptation stimuli until the point of subjective equality (PSE) is reached. The size of the after-effect is then given by the ratio of the relevant feature between the two test stimuli at the PSE. One of the methods we have employed to reveal the spatial feature(s) that is being adapted is to use adaptation pairs that differ in shape-frequency or shape-amplitude, but in which a given 'test' feature is set to be equal in the two adaptors. The logic is that if it that test feature is the one being adapted then the SFAE/SAAE will be eliminated. Other methods employed include the use of square-wave-shaped contours and contours consisting of fragments of a sine-wave-shaped contour. The features we have tested are local orientation, average unsigned curvature, periodicity/density, shape-amplitude and local curvature. Our results have enabled us to identify the spatial feature underlying the SFAE and SAAE, and to suggest the stage in shape processing at which the after-effects probably occur.

2. General methods

2.1. Observers

The two authors (E.G. and F.K.) and two undergraduate volunteers (K.W. and A.B.), who were both naive observers, participated in the study. All subjects had normal or corrected-to-normal visual acuity.

2.2. Stimuli

The stimuli were generated by a VSG2/5 video-graphics card (Cambridge Research Systems) with 12-bits contrast resolution, presented on a calibrated, gamma-corrected Sony Trinitron monitor, running at 120 Hz frame rate and with a spatial resolution of 1024×768 pixels. The mean luminance of the monitor was 42 cd/m^2.

Example stimuli are shown in Fig. 1. Adaptation and test stimuli consisted of pairs of 2D sine-wave-shaped contours, except in the experiment using square-wave test contours in which only one adaptor was used. Unless otherwise stated, the adaptor pair for the SFAE consisted of contours with a shape-amplitude of 0.43 deg and shape frequencies of 0.25 and 0.75 c/deg, giving a geometric mean shape-frequency of 0.43 c/deg. For the SAAE, the shape-frequency of the adaptor pair was 0.43 c/deg, while the shape-amplitudes were 0.25 and 0.75 deg (geometric mean 0.43 deg). The two adaptors/tests were presented in the center of the monitor 3.5 deg above and below the fixation marker. The cross-sectional luminance profile of the contours was odd-symmetric and was generated according to a first derivative of a Gaussian function:

$$L(d) = L_{\text{mean}} \pm L_{\text{mean}} \cdot C \cdot \exp(0.5) \cdot (d/\sigma) \cdot \exp[-(d^2)/(2\sigma^2)]$$

where d is the distance from the midpoint of the contour's luminance profile along a line perpendicular to the tangent, L_{mean} is mean luminance of 42 cd/m^2, C contrast and σ the space-constant. C was set to 0.5 and σ to 0.044 deg for all experiments. Our contours were designed to have a constant cross-sectional width, and the method we used to achieve this is described in Gheorghiu and Kingdom (2006a).

2.3. Procedure

Each session began with an initial adaptation period of 90 s, followed by a repeated test of 0.5 s duration interspersed with top-up adaptation periods of 2.5 s. During the adaptation period, the shape-phase of the contour was randomly changed every 0.5 s in order to prevent the formation of afterimages and to minimize the effects of local orientation adaptation. The presentation of the test contour was signaled by a tone. The shape-phase of the test contour was also randomly assigned in every test period. The display was viewed in a dimly lit room at a viewing distance of 100 cm. Subjects were required to fixate on the marker placed between each pair of contours for the entire session. A head and chin rest helped to minimize head movements.

A staircase method was used to estimate the PSE. For the SFAE the geometric mean shape-frequency of the two test contours was held constant at 0.43 c/deg while the computer varied the relative shape-frequencies of the two tests in accordance with the subject's response. At the start of the test period the ratio of the two test shape-frequencies was set to a random number between 0.33 and 3. On each trial subjects indicated via a button press whether the upper or lower test contour had the higher perceived shape-frequency. The computer then changed the

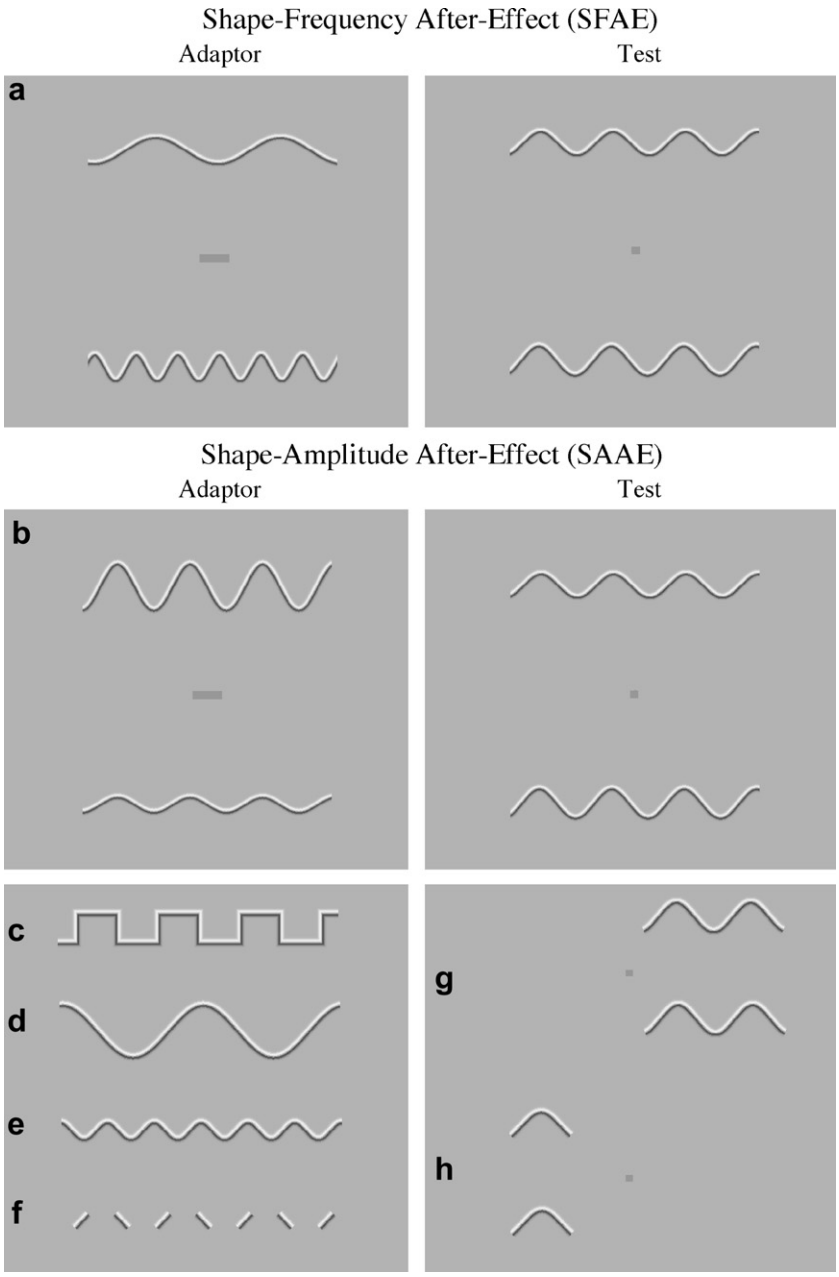

Fig. 1. Stimuli used in the experiments. One can experience (a) the shape-frequency after-effect (SFAE) and (b) the shape-amplitude after-effect (SAAE) by moving one's eyes back and forth along the markers located midway between the pair of adapting contours (left) for about 90 s, and then shifting one's gaze to the middle of the test contours (right). (c)–(h) Example contours used in the experiments. (c) Square-wave-shaped contour used in Experiment 1; (d) and (e) contours with the same average unsigned curvature, as used in Experiment 2; (f) array of oriented elements as used in Experiment 3; (g) and (h) example test contour pairs used in Experiment 5. The two pairs are shown in different horizontal positions within the 8 deg stimulus window. (g) Test contour pair 3.16 deg width in—cosine phase; (h) test contour pair 1.4 deg width in +cosine phase.

ratio of test shape-frequencies by a factor of 1.06 for the first five trials and 1.015 thereafter, in a direction opposite to that of the response, i.e. towards the PSE. The session was terminated after 25 trials. Six measurements were made for each condition, three in which the upper adaptor had the higher shape-frequency and three in which the lower adaptor had the higher shape-frequency. The shape-frequency ratio at the PSE was calculated as the geometric mean shape-frequency ratio of the test that followed the lower shape-frequency adaptor to the test that followed the higher shape-frequency adaptor, averaged across the last 20 trials. In addition we measured for each condition the shape-frequency ratio at the PSE in the absence of the adapting stimulus (the no-adaptor condition). To obtain an estimate of the size of the SFAE we calculated the difference between the log with-adaptor shape-frequency ratio at the PSE and the mean log no-adaptor shape-frequency ratio at the PSE, for each with-adaptor measurement. We then calculated the mean and standard error of these differences across measurements. These standard errors are the ones shown in the graphs.

The procedure for measuring the SAAE followed the same principle as for the SFAE. The computer varied the relative shape-amplitudes of the two tests in accordance with the subject's response, while the geometric mean shape-amplitude of the two test contours was held constant at 0.43 deg.

3. Experiment 1: local orientation?

The tilt after-effect (TAE) is the phenomenon in which prolonged adaptation to an oriented stimulus, such as a line or grating causes a shift in the apparent orientation of a subsequently presented stimulus in a direction away from that of the adaptation stimulus (Coltheart, 1971; Gibson, 1933; Gibson & Radner, 1937; Magnussen & Johnsen, 1986; Magnussen & Kurtenbach, 1979, 1980a, 1980b; Mitchell & Muir, 1976; Paradiso, Shimojo, & Nakayama, 1989; Rosness, Magnussen, & Nordby, 1994; Wenderoth & Johnstone, 1988). It is widely believed that the TAE is caused by a change, either from fatigue or lateral inhibition, in the shape of the response distribution of orientation-selective neurons (Coltheart, 1971; Dragoi, Sharma, & Sur, 2000, 2001; Ganz, 1966; Koehler & Wallach, 1944).

The SFAE occurs even though the shape-phase of the adaptation contour is randomly changed every half second during the adaptation period, and the shape-phase of the test contour randomly changed for each presentation. This might be taken to imply that the SFAE cannot be mediated by the TAE, because the orientation content of the adaptor at any one visual location is constantly changing, and therefore any local TAEs will tend to cancel each other out. However, an examination of the geometrical relationships between sine-wave-shaped adaptors and tests shows that this assumption is questionable. As an illustration, Fig. 2a shows a short segment of a test in just two of the possible phases relative to the peak of a lower-in-shape-frequency adaptor: $-\pi/2$ (phase A) and $+\pi/2$ (phase B). If one considers just the near-straight portions of the contours that cross the d.c., one can see how opposite TAEs would be produced for the test in these two phase positions. However, the magnitudes of the TAEs will presumably be different: the TAE at phase A will be smaller than at phase B because the orientations of adaptor and test at phase B are more similar and the TAE is known to peak at an adaptor-test orientation difference of only about 15 deg (Gibson & Radner, 1937; Paradiso et al., 1989; Wenderoth & Johnstone, 1988). Although we have considered only two phases, we have chosen the ones that will produce the biggest difference in the magnitude and direction of the TAE, and it follows that the net result across all relative phases of adaptor and test will be a slight shift in the perceived orientation of the test towards vertical. By the same argument a higher-in-shape-frequency adaptor will cause a net shift in the test orientations towards horizontal. Although intuitively such changes in the perceived orientation of the contour around the d.c. would be expected to produce distortions in the perceived shape rather than perceived periodicity of the test contour, one cannot rule out that perceived periodicity might also be affected.

The above argument also applies to the SAAE. In fact one might expect shifts in local perceived orientation to

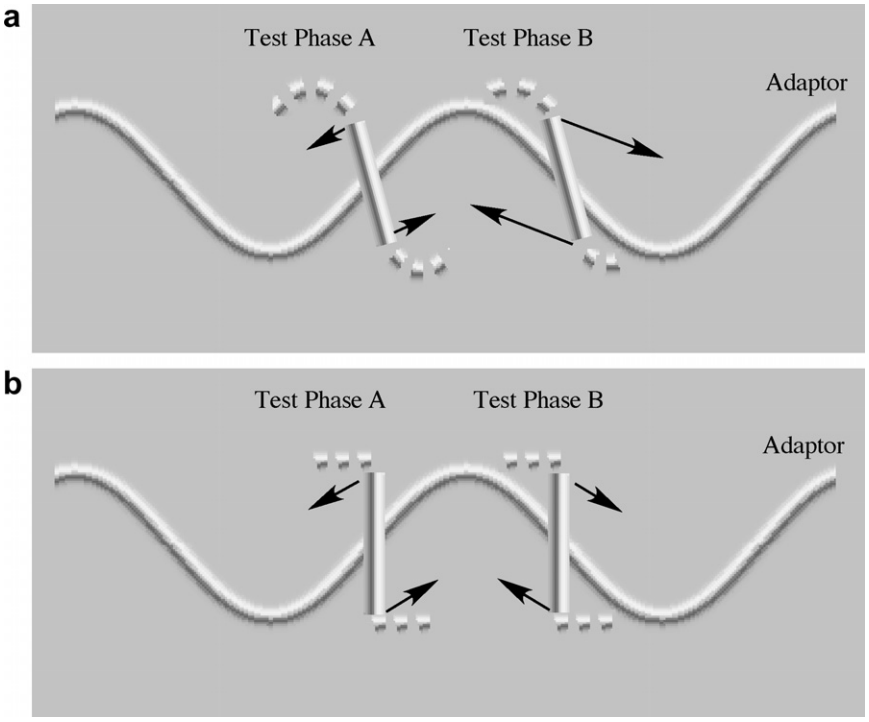

Fig. 2. How orientation adaptation, i.e. the tilt after-effect (TAE), might underlie the SFAE and SAAE. (a) Part of a sine-wave-shaped contour adaptor overlaid by a short segment of a higher-in-shape-frequency test contour in two phases, $-\pi/2$ (phase A) and $+\pi/2$ (phase B), relative to the peak of the adaptor. Opposite TAEs would be produced for the test at the two phase positions, but their magnitudes would be different and hence would not cancel. (b) The analogous situation for a square-wave-shaped test. In this case the TAEs will always be equal and opposite for the two phase positions, and therefore will cancel. See text for further details.

impact perceived shape-amplitude even more than perceived shape-frequency, because shape-amplitude is a feature orthogonal in orientation to the periodicity of the stimulus.

Consider now Fig. 2b, which shows the analogous situation for a square-wave-shaped test in the same two relative phase positions. In this case the TAEs will always be equal and opposite for the two phase positions. It follows that we would not expect any net shift in perceived local orientation and hence, if local orientation caused the SFAE and SAAE, no shift in either perceived shape-frequency or perceived shape-amplitude. Thus, we can make the following prediction. If the SFAE and SAAE obtained using sine-wave-shaped contours result from local orientation adaptation, the after-effects should disappear when the test is square-wave-shaped. On the other hand if the after-effects result from something other than orientation adaptation, we should expect significant sized after-effects with square-wave-shaped tests.

To obtain a detailed comparison of the after-effects between sine-wave-shaped and square-wave-shaped tests we used the single-adaptor method. This method is different from the one described in Sections 2.2 and 2.3 in that a single rather than a pair of adaptors was used. The adaptor is presented either above or below fixation, and the test was presented in the same location as the adaptor. The comparison contour, which was adjusted during the test period to obtain the PSE, was presented in the other visual hemifield to that of the test. For the SFAEs adaptor and test had a shape-amplitude of 0.5 deg. The test was fixed in shape-frequency at 0.5 c/deg, and the adaptors were set to one of 10 values: 0, 0.125, 0.177, 0.25, 0.354, 0.5, 0.707, 1, 1.414 and 2 c/deg. For the SAAEs adaptor and test had a shape-frequency of 0.5 c/deg. The test was set to a shape-amplitude of 0.5 deg, and the adaptors were set to one of 11 values: 0, 0.125, 0.177, 0.25, 0.354, 0.5, 0.707, 1, 1.414, 2 and 3 deg. The procedure and subject's task was as described in Section 2.3. For this experiment, the shape-frequency ratio at the PSE was calculated as the mean geometric ratio of test to comparison shape-frequencies over the last 20 trials. The estimate of the SFAE and SAAE was calculated as described in Section 2.3.

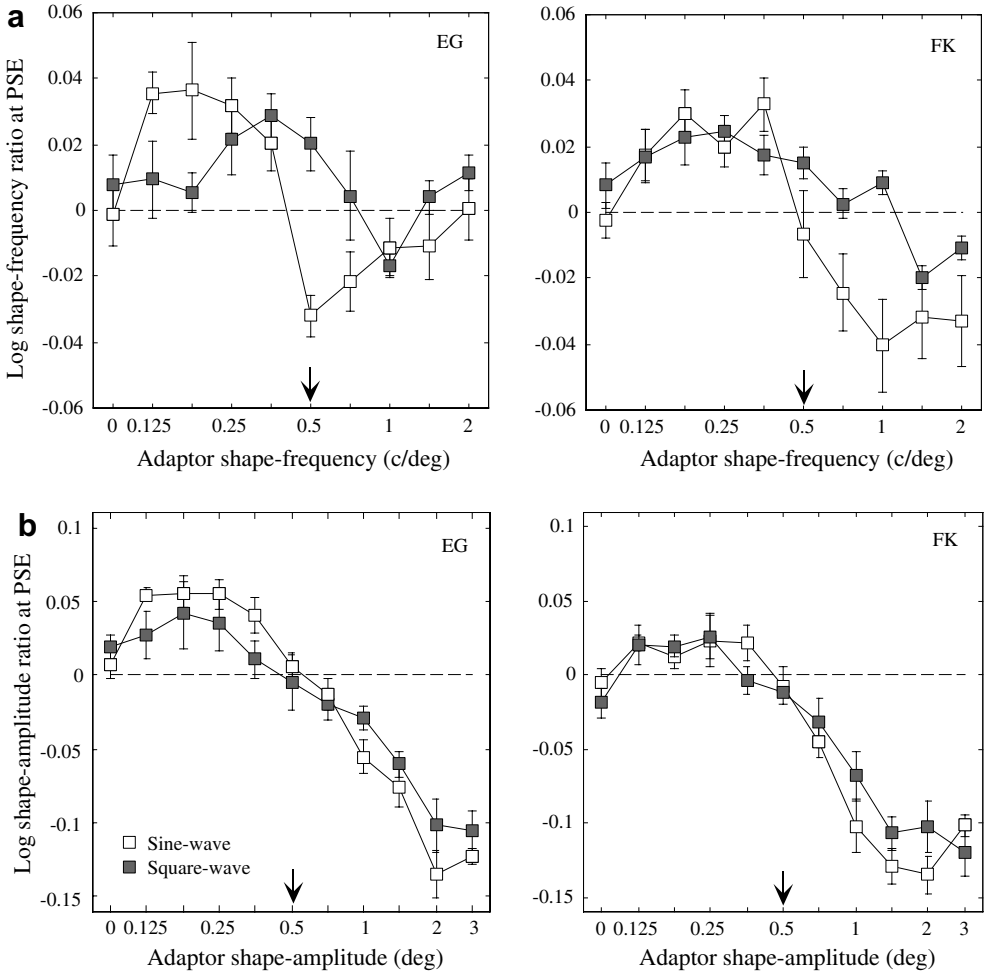

Fig. 3. Results for Experiment 1. (a) SFAEs as a function of adaptor shape-frequency; (b) SAAEs as a function of adaptor shape-amplitude. Open symbols are for sine-wave-shaped test, closed symbols square-wave-shaped tests. Data are shown for two subjects. The arrow indicates the test shape-frequency in (a) and the test shape-amplitude in (b). Error bars are standard errors of the mean difference between the with-adaptor and no-adaptor conditions calculated across six measurements (see text for details).

Fig. 3 shows (a) SFAEs as a function of adaptor shape-frequency and (b) SAAEs as a function of adaptor shape-amplitude, for both sine-wave-shaped (open symbols) and square-wave-shaped (gray filled symbols) test contours. Note first that in all but the square-wave SFAEs, the after-effect reverses direction as the adaptor shape-frequency (or shape-amplitude) switches from being lower to higher than the test, which is shown by the arrow. This shows that the after-effects are bi-directional: positive values indicate that lower shape-frequencies (or shape-amplitudes) cause higher shape-frequencies (or shape-amplitudes) to look higher, negative values that higher shape-frequencies (or shape-amplitudes) cause lower shape-frequency (or shape-amplitudes) to look lower. Note however that for the SAAEs in Fig. 3b, although the effect is bi-directional, there is an asymmetry in the size of SAAEs, with positive shifts being smaller than negative shifts. We will return in the Discussion to consider the possible reasons for this asymmetry, as well as to the reason why the square-wave SFAEs appear translated along the x axis compared to the sine-wave SFAEs. Another interesting feature of the data, and one that we will find consistently throughout the experiments reported here, is that peak SAAEs are on average about 0.1 log units (1.26×) greater than peak SFAEs (note the y axes are differently scaled). Finally, and for the present purpose this is the critical finding, the after-effects are similar in magnitude for both sine-wave-shaped and square-wave-shaped tests. Based on the arguments given above, this suggests that the TAE is not the underlying cause of either the SFAE or SAAE.

4. Experiment 2: average unsigned curvature?

In this experiment, we investigate whether average unsigned curvature underlies the SFAE and SAAE. The curvature at any point on a contour is given by the second derivative of the function describing the contour's shape, and for a sine-wave-shaped contour the average curvature across a whole cycle is zero, because both positive and negative curvatures are present. However, if the sign of curvature is discarded, the average curvature is proportional to the product of shape-frequency and shape-amplitude. Average unsigned curvature can be thought of as the average 'curviness' of the contour. Two contours with the same shape-frequency but different shape-amplitude, or vice-versa, will have different average unsigned curvatures, and thus average unsigned curvature could be the spatial feature underlying the SFAE and SAAE. It follows that if one used pairs of adaptors that differed in both shape-frequency and shape-amplitude, such that they had the same average unsigned curvature, we should expect the after-effects to disappear. An example of such a pair is shown in Fig. 1d and e. Another prediction is that even if the two adaptors differ only in shape-frequency (i.e. have the same shape-amplitude) after-effects in both shape-frequency and shape-amplitude will be observed, and that even if the two adaptors differ only in shape-amplitude (same shape-frequency) after-effects in both shape-amplitude and shape-frequency will be observed.

To test these predictions we used pairs of sine-wave-shaped contour adaptors with (i) different shape-amplitudes (0.25 and 0.75 deg) but the same shape-frequency (0.43 c/deg)—the shape-amplitude-only condition; (ii) different shape-frequencies (0.25 and 0.75 c/deg) but the same shape-amplitude (0.43 deg)—the shape-frequency-only condition; (iii) different shape-amplitudes (0.25 and 0.75 deg) and different shape-frequencies (0.75 and 0.25 c/deg), such that average unsigned curvature was the same for the two adaptors—the equal curvature condition. For each of the three adaptor conditions we measured both SFAEs and SAAEs, making six conditions in total.

Fig. 4 shows SAAEs as gray filled bars and SFAEs as white bars for all three adaptor conditions. The results show (a) equal-sized SAAEs for the shape-amplitude-only

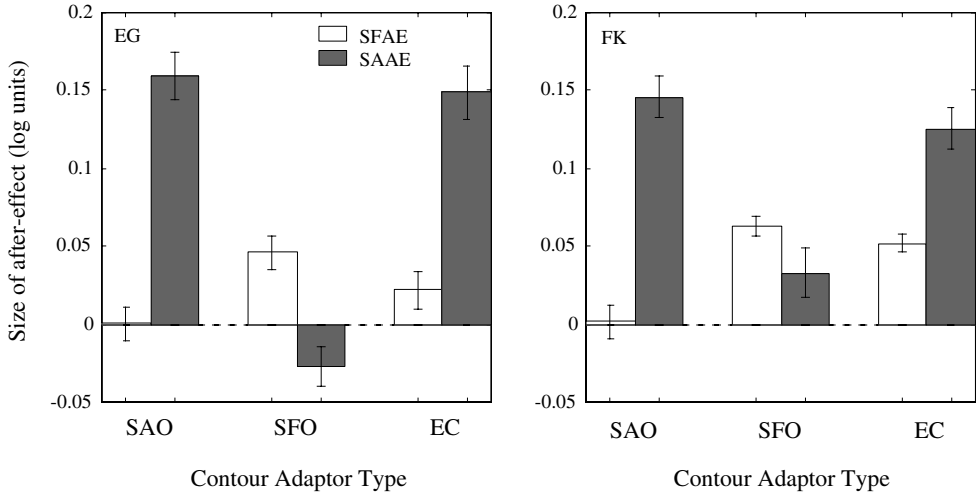

Fig. 4. Results for Experiment 2. SAAEs (gray bars) and SFAEs (white bars) for three adaptor conditions: (i) SAO, shape-amplitude-only condition; (ii) SFO, shape-frequency-only condition; (iii) EC, equal curvature condition.

and equal-curvature conditions (the two tall gray bars); (b) nearly equal-sized SFAEs for shape-frequency-only and equal-curvature conditions; (c) zero SFAEs for the shape-amplitude-only condition; (d) relatively small, and in opposite directions for the two subjects, SAAEs for the shape-frequency-only condition.

These results do not support any of the predictions made above, and show unequivocally that average unsigned curvature is not the spatial feature underlying the SAAE and SFAE.

5. Experiment 3: periodicity and/or density (SFAE only)?

Here, we investigate whether periodicity and/or density underlies the SFAE. Periodicity and density are co-variants in contours that vary in shape-frequency. Density after-effects have previously been shown for a variety of textured stimuli (Durgin, 1996, 2001; Durgin & Huk, 1997; Durgin & Proffitt, 1996). The adaptors we used were sine-wave-shaped contours, but there were two types of tests: (i) sine-wave-shaped contours, and (ii) an array of oriented elements, as shown in Fig. 1f. The array of oriented elements was obtained by 'chopping off' the peaks and troughs of a sine-wave-shaped contour with a shape-frequency of 0.43 c/deg and shape-amplitude of 0.43 deg, leaving near-straight elements with an amplitude of 0.215 deg. The orientations of the elements were not however varied during the test procedure; only their spacing was varied. The rationale for using the array of oriented elements was that the elements had the same average orientation and arrangement as those parts of the adaptors that were likely to be involved in the adaptation of periodicity/density. The two sine-wave-shaped adaptors had shape frequencies of 0.25 and 0.75 c/deg and a shape-amplitude of 0.43 deg. The task for the subject for both the element-array and sine-wave-shaped tests was the same as in previous experiments: to compare the perceived spatial frequency of the two tests.

If SFAEs result from adaptation to periodicity/density, we expect near-equal-sized after-effects for the conventional sine-wave-shaped and element-array tests. Fig. 5 shows SFAEs for the two test conditions. SFAEs for the element-array tests were close to zero, suggesting that periodicity/density is not the feature being adapted in the SFAE.

6. Experiment 4: shape-amplitude (SAAE only)?

In this experiment, we examine whether shape-amplitude per se underlies the SAAE. By shape-amplitude per se, we mean the presence of contour energy between the peaks and troughs of the waveform. If shape-amplitude per se underlies the SAAE, then the relative *shape frequencies* of adaptor and test should not matter. To test this idea, we used pairs of sine-wave-shaped contour adaptors with shape-amplitudes 0.25 and 0.75 deg (geometric mean 0.43 deg) but whose shape-frequency was varied, while the test shape-frequency was fixed at one of two values: 0.25 and 1.0 c/deg. There were nine values of adaptor shape-frequency: 0.125, 0.178, 0.25, 0.353, 0.5, 0.707, 1.0, 1.414 and 2 c/deg. The task and procedure are described in Section 2.3.

Fig. 6 shows SAAEs as a function of adaptor shape-frequency for both the lower 0.25 c/deg (open symbols) and higher 1.0 c/deg (gray filled symbols) test shape-frequencies. The results show unequivocally that the SAAE is tuned to shape-frequency; both functions peak when the shape frequencies of adaptor and test are the same. Thus we conclude that shape-amplitude per se is not the underlying cause of the SAAE.

7. Experiment 5: local curvature?

In this experiment, we examine whether local curvature underlies the SFAE and SAAE. If local curvature underlies the two after-effects, then we would expect the after-effect to reach a maximum when the largest fragment of the test

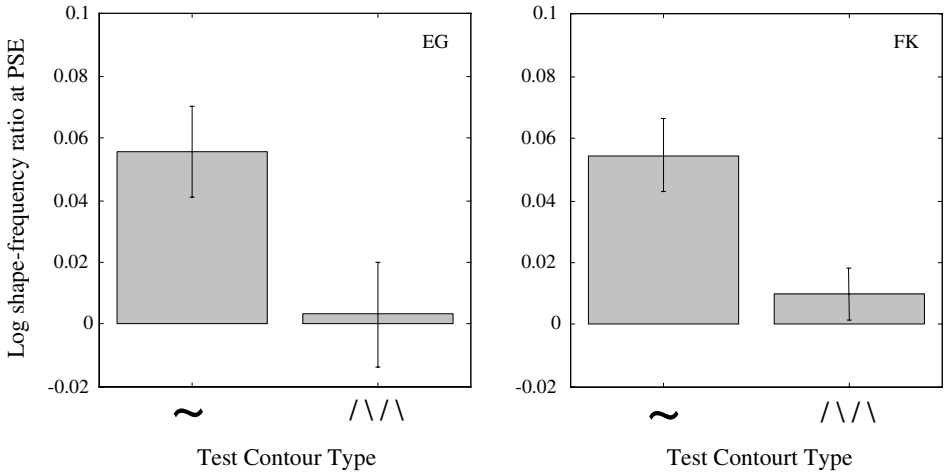

Fig. 5. Results for Experiment 3. SFAEs for (i) sine-wave-shaped tests and (ii) array of oriented element tests.

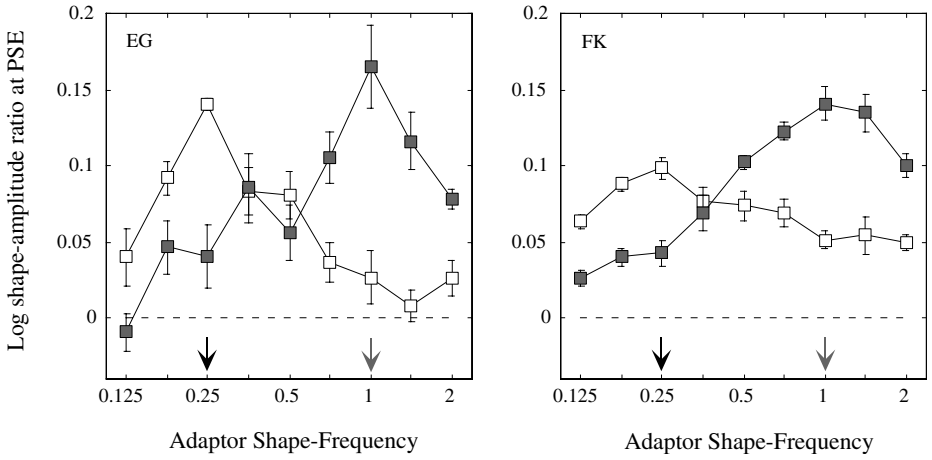

Fig. 6. Results for Experiment 4. SAAEs as a function of adaptor shape-frequency for 0.25 c/deg (open symbols) and 1.0 c/deg (gray filled symbols) test shape-frequencies. The arrows indicate the two test shape-frequencies.

that had a constant sign of curvature was presented. To test this idea, we varied the width of the test contour while keeping the adapting contour constant at 8 deg. We used nine values of test width for the SFAE: 0.5, 0.707, 1.0, 1.414, 2.0, 2.828, 4.0, 5.656 and 8.0 deg, and nine values of test width for the SAAE: 0.676, 0.920, 1.254, 1.707, 2.325, 3.167, 4.313, 6.168 and 8.0 deg. On each test presentation the two test contours were presented at the same randomly selected horizontal position within the 8 deg window, with the constraint that the whole of the test contour fragment should be visible. The phase of the test contour pair was set to ±cosine with respect to its centre. Example test contour pairs with different widths and in different horizontal positions are shown in Fig. 1g and h. Task and procedure were as before.

Fig. 7 shows SFAEs (open symbols) and SAAEs (gray filled symbols) as a function of test width for three subjects. For this experiment, which turned out to produce the key finding, we tested two naïve subjects as well as one of the authors. The results indicate that as test width increases from zero, both SFAEs and SAAEs show a steep rise to a maximum at about 1.4 deg, after which all three subjects for the SFAE, but just one subject for the SAAE show a steady decline. A width of 1.4 deg corresponds to 0.55 cycles (see example in Fig. 1h), indicating that both the SFAEs and SAAEs reached a maximum when the test contour was gated down to just half-a-cycle centered on the peak or trough. We attempted to test whether the ±cosine phase was the optimal phase for the half-cycle stimulus by comparing the results with measurements made using ±sine tests. However for ±sine tests up to just over half-a-cycle the stimulus appeared as a near-straight tilted line, and the task of comparing either the shape-frequency or shape-amplitude of the two test lines felt invalid since the most prominent dimension appearing to vary during the test period was orientation. We therefore suggest that ±cosine is the optimal shape phase for eliciting the SFAE and SAAE in half-cycle fragments of a sinusoidal contour.

8. General discussion

Having rejected the idea that the SFAE and SAAE are mediated by adaptation to (a) local orientation, (b) average unsigned curvature, (c) periodicity/density (SFAE only) and (d) shape-amplitude (SAAE only), we found evidence that local curvature is the spatial feature underlying both after-effects. Both after-effects reached a maximum (or asymptoted) when a half-cycle of the sine-wave test contour, in positive or negative cosine phase, was presented. This suggests that the SFAE and the SAAE are mediated by intermediate-level shape-encoding mechanisms involved in coding the shapes of contour segments that have a constant sign of curvature. Consistent also with a local curvature explanation is our finding in Experiment 4 that the SAAE was tuned to shape-frequency, since only when the shape-frequencies of the adaptors and tests are the same is the mean curvature of the adaptor pair the same as the mean curvature of the test pair.

In Experiment 2, we showed that adaptation pairs that differed only in shape-frequency produced almost no shape-amplitude after-effect, and adaptation pairs that differed only in shape-amplitude produced no shape-frequency after-effect. This suggests that the SFAE and SAAE are largely independent after-effects, even if they act on the same half-cycle portions, i.e. curves, of the stimulus. Specifically our results suggest that the SAAE operates on the sag (sagitta) of a curve (defined as the maximum deviation from linearity) whereas the SFAE operates on the cord of a curve. In short, the two principle axes of a symmetric curve, the sag and cord, appear to be separately adaptable.

We mentioned in Section 1 how Blakemore and Over (1974) showed that local orientation adaptation underlies the effect in which adaptation to a curved line results in a straight line appearing curved in the opposite direction. Their conclusion was based on the observation that the after-effect disappeared if the subject moved his/her eyes back and forth along the cord of the curve during adapta-

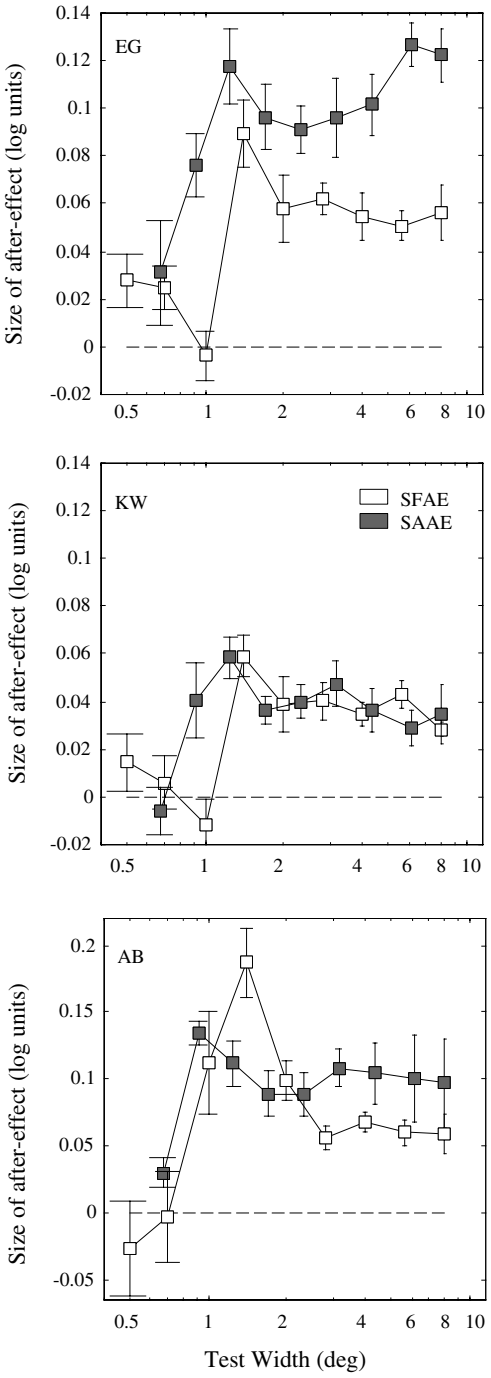

Fig. 7. Results for Experiment 5. SFAEs (open symbols) and SAAEs (gray filled symbols) as a function of contour test width for three subjects. SFAEs and SAAEs peak at about 1.4 deg width, corresponding to 0.55 cycles i.e. just over half-a-cycle of shape modulation centered on the peak or trough (see Fig. 1h).

tion. In other words this form of the curvature after-effect was dependent on adaptor phase. To our knowledge, the SFAE and SAAE are the first examples of curvature after-effects that are not dependent on adaptor phase, and, as we have demonstrated, do not appear to be caused by orientation adaptation.

One interesting feature of the results of Experiment 5, in which we varied the width of the test contour, is that in two out of the three subjects there was a systematic decline in the after-effect with width beyond the half-cycle peak in the SFAE but not SAAE. One explanation for this is that with the SFAE, the visual system is confronted with conflicting information, on the one hand the accumulative effect of multiple local distortions, on the other the veridical representation of local position (see Georgeson (1979) and Meese & Georgeson (1996) for a discussion of this issue with respect to spatial-frequency and orientation adaptation). If we assume that each half-cycle is perceptually altered in width following adaptation, then, if the distortions were cumulative, there would be a substantial change in the width of the whole contour. This would entail shifting the positions of each half-cycle by an amount proportional to the distance of each half-cycle from some anchor point. This would conflict however with the presumably veridical (albeit sloppy) representation of the position of each half-cycle. The visual system might therefore restrict the impact of each local distortion to prevent the cumulative effect conflicting with the positional information, and the amount of restriction would be proportional to the number of local distortions. The result would be the steady decline in the SFAE with the number of cycles after the peak in the after-effect. No such conflict would be expected with the SAAE, as in this case the periodicity is orthogonal in orientation to the feature being adapted.

Another interesting feature of the data concerns the square-wave test results in Experiment 1 (Fig. 3). For the SAAE the square-wave and sine-wave data are very similar, crossing the zero-after-effect horizontal line at the same point. However with the SFAE the square-wave data appear shifted to the right of the sine-wave data by about a factor of 2 with the result that few data points fall below the zero line. A possible reason for this is that the visual system represents the square-wave contour as a series of local curvatures each with its own width (cord length) and height (sag). The presence of adaptable shape harmonics would cause the adaptor shape-frequency at which the after-effect switches from positive to negative to be shifted along the adaptor shape-frequency axis. For example if only the fundamental (0.5 c/deg) and third harmonic (1.5 c/deg) shapes were adapted, probably of course by different amounts, the cross over would be shifted to a value somewhere between 0.5 and 1.5 c/deg, as we find (Fig. 3). This result therefore throws up the tantalizing possibility that complex shapes might be represented in a manner analogous to a local Fourier decomposition, but in which the basis functions are local curvatures rather than sinusoidal shapes. We are currently conducting experiments to test this idea.

Another interesting feature of the data from Experiment 1 is the asymmetry between negative and positive SAAEs (Fig. 3b); higher-in-shape-amplitude adaptors are more effective at shifting tests to lower perceived amplitudes than lower-in-shape-amplitude adaptors are at shifting tests to higher perceived amplitudes. At the moment we do not have a good explanation for his asymmetry, though one

possible explanation is that the transducer function for sag is an accelerating function, resulting in disproportionate strengths for higher compared to lower sags.

The idea that there exist specialized mechanisms for the detection and encoding of curvature has a long history, and will not be reviewed in detail here. Suffice to say that although a considerable amount of psychophysical evidence is *consistent* with the operation of specialized curvature-sensitive mechanisms (e.g. Dobbins, Zucker, & Cynader, 1987, 1989; Koenderink & Richards, 1988; Wilson, 1986; Wilson & Richards, 1989; Zetzsche & Barth, 1990; and see references below), there is little direct psychophysical support for specialized curvature encoders in human vision. Neurophysiological studies on the other hand have revealed neurons in area V4 that are selective for parts of shapes with constant sign of curvature (Pasupathy & Connor, 1999, 2001, 2002). Therefore, if we are correct that the SFAE and SAAE are mediated by mechanisms selective for sinusoidal half-cycles in cosine phase, V4 is the best candidate area for these after-effects.

Although the evidence reported here is strongly indicative of the presence of curvature encoding mechanisms, it does not tell us about the underlying mechanism for curvature encoding. Several authors have proposed mechanisms for curvature detection and discrimination (Koenderink & Richards, 1988; Kramer & Fahle, 1996; Poirier & Wilson, 2006; Watt & Andrews, 1982; Wilson & Richards, 1989). For example Tyler (1973), Wilson and Richards (1989) and Kramer and Fahle (1996) have proposed that low curvatures are detected by comparing orientations at different points along the contour using orientation-selective filters. For higher curvatures, suggestions have included end-stopped neurons (Dobbins et al., 1987, Dobbins, Zucker, & Cynader, 1989; Koenderink & Richards, 1988; Wilkinson et al., 1998), and the combination by AND-gating (i.e. multiplication) of the responses of neurons with different orientation preferences (Poirier & Wilson, 2006; Zetzsche & Barth, 1990). However it is important to bear in mind that models for curvature detection and discrimination do not necessarily provide an account of how curvature is represented in the visual system, which presumably involves an analysis of the distribution of responses from detectors tuned to different curvatures, as with orientation coding (Coltheart, 1971; Dragoi, Rivadulla, & Sur, 2001; Ganz, 1966;Koehler & Wallach, 1944). We are currently using the SFAE and SAAE to attempt to determine how curvature is encoded by the human visual system.

Acknowledgments

This research was supported by a Natural Sciences and Engineering Research Council of Canada (NSERC) Grant # OGP01217130 given to F.K.

References

Anderson, N. D., Habak, C., Wilkinson, F., & Wilson, H. R. (2005). Evaluating curvature aftereffects with radial frequency contours. *Journal of Vision, 5*(7), 209, Abstract.

Anderson, N. D., & Wilson, H. R. (2005). The nature of synthetic face adaptation. *Vision Research, 45*, 1815–1828.

Blakemore, C., & Over, R. (1974). Curvature detectors in human vision? *Perception, 3*(1), 3–7.

Coltheart, M. (1971). Visual feature-analyzers and after-effects of tilt and curvature. *Psychological Review, 78*(2), 112–121.

DeValois, R. L., & DeValois, K. K. (1988). *Spatial Vision*. Oxford University Press.

Dobbins, A., Zucker, S. W., & Cynader, M. S. (1987). Endstopping in the visual cortex as a substrate for calculating curvature. *Nature, London, 329*, 438–441.

Dobbins, A., Zucker, S. W., & Cynader, M. S. (1989). Endstopping and curvature. *Vision Research, 29*(10), 1371–1387.

Dragoi, V., Rivadulla, C., & Sur, M. (2001). Foci of orientation plasticity in visual cortex. *Nature, 411*(6833), 80–86.

Dragoi, V., Sharma, J., & Sur, M. (2000). Adaptation-induced plasticity of orientation tuning in adult visual cortex. *Neuron, 28*(1), 287–298.

Durgin, F. H. (1996). Visual aftereffects of texture density contingent on color of frame. *Perception & Psychophysics, 58*(2), 207–223.

Durgin, F. H. (2001). Texture contrast after-effects are monocular; texture density aftereffects are binocular. *Vision Research, 41*(20), 2619–2630.

Durgin, F. H., & Huk, A. C. (1997). Texture density aftereffects in the perception of artificial and natural textures. *Vision Research, 37*(23), 3273–3282.

Durgin, F. H., & Proffitt, D. R. (1996). Visual learning in the perception of texture: simple and contingent aftereffects of texture density. *Spatial Vision, 9*(4), 423–474.

Gallant, J. L., Braun, J., & Van Essen, D. C. (1993). Selectivity for polar, hyperbolic and Cartesian gratings in macaque visual cortex. *Science, 259*(5091), 100–103.

Gallant, J. L., Connor, C. E., Rakshit, S., Lewis, J. W., & Van Essen, D. C. (1996). Neural responses to polar, hyperbolic, and Cartesian gratings in area V4 of the macaque monkey. *Journal of Neurophysiology, 76*(4), 2718–2739.

Ganz, L. (1966). Mechanisms of figural after-effects. *Psychological Review, 73*, 128–150.

Georgeson, M. A. (1979). Spatial Fourier analysis and human vision. In N. S. Sutherland (Ed.), Tutorial essays in psychology (Vol. 2, Chap. 2, pp. 39–88). Hillsdale, N.J.: Erlbaum.

Gheorghiu, E., & Kingdom, F. A. A. (2006a). Luminance-contrast properties of contour-shape processing revealed through the shape-frequency after-effect. *Vision Research, 46*(21), 3603–3615.

Gheorghiu, E., & Kingdom, F. A. A. (2006b). Luminance-contrast properties of contour-shape processing revealed through adaptation. *Journal of Vision, 6*(6), 338.

Gibson, J. J. (1933). Adaptation. aftereffect and contrast in the perception of curved lines. *Journal of Experimental Psychology, 20*, 453–467.

Gibson, J. J., & Radner, M. (1937). Adaptation, aftereffect and contrast in the perception of tilted lines. I. Quantitative studies. *Journal of Experimental Psychology, 20*, 453–467.

Gross, C. G. (1992). Representation of visual stimuli in inferior temporal cortex. *Philosophical Transactions of the Royal Society of London. Series B, Biological Sciences, 29: 335*(1273), 3–10, Review.

Habak, C., Wilkinson, F., Zahker, B., & Wilson, H. R. (2004). Curvature population coding for complex shapes in human vision. *Vision Research, 44*, 2815–2823.

Hess, R. F., Wang, Y. Z., & Dakin, S. C. (1999). Are judgments of circularity local or global? *Vision Research, 39*(26), 4354–4360.

Hubel, D. H., & Wiesel, T. N. (1968). RFs and functional architecture of monkey striate cortex. *Journal of Physiology, 195*, 215–243.

Ito, M., Fujita, I., Tamura, H., & Tanaka, K. (1994). Processing of contrast polarity of visual images in inferotemporal cortex of the macaque monkey. *Cerebral cortex, 4*(5), 499–508.

Keeble, D. R. T., & Hess, R. F. (1999). Discriminating local continuity in curved figures. *Vision Research, 39*, 3287–3299.

Kingdom, F. A. A., & Gheorghiu, E. (2006). On the mechanisms for contour-shape after-effects. *Journal of Vision, 6*(6), 339.

Kingdom, F. A. A., & Prins, N. (2005a). Different mechanisms encode the shapes of contours and contour-textures. *Journal of Vision, 5*(8), 463.

Kingdom, F. A. A., & Prins, N. (2005b). Separate after-effects for the shapes of contours and textures made from contours. *Perception, 34*(Suppl.), 92, Abstract.

Koehler, W., & Wallach, H. (1944). Figural after-effects: an investigation of visual responses. *Proceedings of the American Philosophycal Society, 88*, 306–335.

Koenderink, J. J., & Richards, W. (1988). Two-dimensional curvature operators. *Journal of the Optical Society of America A, 5*, 1136–1141.

Kramer, D., & Fahle, M. (1996). A simple mechanism for detecting low curvatures. *Vision Research, 36*(10), 1411–1419.

Levi, D. M., & Klein, S. A. (2000). Seeing circles: what limits shape perception? *Vision Research, 40*(17), 2329–2339.

Loffler, G., Wilson, H. R., & Wilkinson, F. (2003). Local and global contributions to shape discrimination. *Vision Research, 43*, 519–530.

Magnussen, S., & Johnsen, T. (1986). Temporal aspects of spatial adaptation. A study of the tilt after-effect. *Vision Research, 26*(4), 661–672.

Magnussen, S., & Kurtenbach, W. (1979). A test for contrast-polarity selectivity in the tilt aftereffect. *Perception, 8*(5), 523–528.

Magnussen, S., & Kurtenbach, W. (1980a). Adapting to two orientations: disinhibition in a visual aftereffect. *Science, 207*(4433), 908–909.

Magnussen, S., & Kurtenbach, W. (1980b). Linear summation of tilt illusion and tilt aftereffect. *Vision Research, 20*(1), 39–42.

Meese, T. S., & Georgeson, M. A. (1996). The tilt aftereffect in plaids and gratings: channel codes, local signs and 'patchwise' transforms. *Vision Research, 36*(10), 1421–1437.

Mitchell, D. E., & Muir, D. W. (1976). Does the tilt after-effect occur in the oblique meridian? *Vision Research, 16*(6), 609–613.

Paradiso, M. A., Shimojo, S., & Nakayama, K. (1989). Subjective contours, tilt aftereffect, and visual cortical organization. *Vision Research, 29*(9), 1205–1213.

Pasupathy, A., & Connor, C. E. (1999). Responses to contour features in macaque area V4. *Journal of Neurophysiology, 82*(5), 2490–2502.

Pasupathy, A., & Connor, C. E. (2001). Shape representation in area V4: position-specific tuning for boundary conformation. *Journal of Neurophysiology, 86*(5), 2505–2519.

Pasupathy, A., & Connor, C. E. (2002). Population coding of shape in area V4. *Nature Neuroscience, 5*(12), 1332–1338.

Poirier, F. J., & Wilson, H. R. (2006). A biological plausible model of human radial frequency perception. *Vision Research, 46*(15), 2443–2455.

Regan, D., & Hamstra, S. J. (1992). Shape discrimination and the judgment of perfect symmetry: dissociation of shape from size. *Vision Research, 32*(10), 1845–1864.

Riggs, L. A. (1973). Curvature as a feature of pattern vision. *Science, 181*(104), 1070–1072.

Rosness, R., Magnussen, S., & Nordby, K. (1994). Spatial vision of the achromat: the tilt after-effect. *Vision Research, 34*(15), 2021–2022.

Stromeyer, C. F., 3rd, & Riggs, L. A. (1974). Curvature detectors in human vision? *Science, 14:184*(142), 1199–1201.

Suzuki, S. (2001). Attention-dependent brief adaptation to contour orientation: a high-level aftereffect for convexity? *Vision Research, 41*, 3883–3902.

Suzuki, S. (2003). Attentional selection of overlapped shapes: a study using brief shape aftereffects. *Vision Research, 43*, 549–561.

Suzuki, S., & Cavanagh, P. (1998). A shape-contrast effect for briely presented stimuli. *Journal of Experimental Psychology: Human Perception and Performance, 24*(5), 1315–1341.

Tanaka, K. (1996). Inferotemporal cortex and object vision. *Annual Review of Neuroscience, 19*, 109–139.

Tyler, C. W. (1973). Periodic vernier acuity. *Journal of Physiology, 228*(3), 637–647.

Watt, R. J., & Andrews, D. P. (1982). Contour curvature analysis: hyperacuities in the discrimination of detailed shape. *Vision Research, 22*(4), 449–460.

Wenderoth, P., & Johnstone, S. (1988). The different mechanisms of the direct and indirect tilt illusions. *Vision Research, 28*(2), 301–312.

Wilkinson, F., Wilson, H. R., & Habak, C. (1998). Detection and recognition of radial-frequency patterns. *Vision Research, 38*, 3555–3568.

Wilson, H. R. (1986). Responses of spatial mechanisms can explain hyperacuities. *Vision Research, 26*(3), 453–469.

Wilson, H. R. (1991). Pattern discrimination, visual filters and spatial sampling irregularity. In J. A. Movshon, M. S. Landy (Eds.): Computational models of visual processing.

Wilson, H. R., & Richards, W. A. (1989). Mechanisms of contour curvature discrimination. *Journal of the Optical Society of America A, 6*, 106–115.

Wilson, H. R., & Richards, W. A. (1992). Curvature and separation discrimination at texture boundaries. *Journal of the Optical Society of America A, 9*(10), 1653–1662.

Zetzsche, C., & Barth, E. (1990). Fundamental limits of linear filters in the visual processing of two-dimensional signals. *Vision Research, 30*(7), 1111–1117.